Influence of the Central Metal Ion on the Desorption Kinetics of a Porphyrin from the Solution/HOPG Interface

Ashish Bhattarai, Kevin Marchbanks-Owens, Ursula Mazur, K. W. Hipps*

Department of Chemistry, Washington State University, Pullman, WA 99164-4630

KW Hipps: hipps@wsu.edu

509-335-3033

Abstract

The changes in desorption kinetics that result from incorporating a metal ion into a porphyrin ring are studied by scanning tunneling microscopy (STM). Desorption studies of cobalt(II) octaethylporphyrin (CoOEP) and free base octaethylporphyrin (H_2OEP) at the 1-phenyloctane/HOPG interface were performed in the 20 °C to 110 °C temperature range.. These studies of mixtures of CoOEP and H_2OEP have shown that the resulting monolayer compositions are stable for more than one year at 20 °C, and are controlled by kinetics to above 100 °C. Quantitative temperature and time dependent surface coverage studies were performed on both CoOEP and H_2OEP at 90 °C, 100 °C, and 110 °C. The desorption activation energies for both porphyrins were found to be $(1.25 \pm 0.05)\times 10^2$ kJ/mol. The rate of desorption and the rate of adsorption for CoOEP are similar to the corresponding rates for H_2OEP, indicating that replacing the central protons with a cobalt ion has only a minor influence on adsorption. Thus, the adsorption strength is dominated by the interactions between the porphyrin ring and HOPG. Comparison of these results with previously published work for the NiOEP/CoOEP system suggests the presence of weak cooperativity in the desorption process. We also found that setting the sample potential to ± 1.5 V relative to earth for periods of the order of an hour had no effect on desorption rates at 50 °C. On the other hand, a large potential difference between tip and sample did produce a significant change in desorption rate.

Introduction

One of the important elements in building modern electronic devices is the use of self-assembled organic adlayers. Self-assembly of organic molecules can be achieved by using different types intermolecular interactions.[1,2] Porphyrins are an important class of organic compounds that readily self-organize on surfaces and because of their chemical and optoelectronic versatility serve as excellent candidates for use in electronic devices such as solar cells[3] and sensors.[4,5] Moreover, porphyrins are abundant in nature and are involved in the complex chemistry of electron transfer,[6,7] photosynthesis in plants,[8] and oxygen binding in heme.

Porphyrins have highly conjugated π-electronic structures and they are strong absorbers of visible light. Thus, they are candidates for use as sensitizers in solar cells.[9-11] They can be chemically modified with different metal cores and diverse substituents at the eight beta and four *meso* positions on the ring periphery to produce a wide range of electronic, optical, structural, and solubility properties. Because, the porphyrin macrocycle has a nearly planar geometry, it likely lies flat on a surface and provides a rigid foundation for any potential surface supported three-dimensional network. The chemical and physical versatility of the porphyrins allow one to design self-assembled monolayers on surfaces with a wide range of properties. At the solution-solid (SS) interface, depending on desorption and adsorption kinetics, self-assembled monolayers might replenish themselves on the surface and could thus form long-range defect free systems. For systems where desorption kinetics are favorable, this allows the nanostructure to *"self-heal"* and can prolong the life of the system.

While various surface sensitive techniques such as XPS, UPS, and UHV-STM have been used to investigate surface processes in vacuum, STM is the primary tool for studying the SS interface at the single molecule level. It provides the adlayer molecular structure at the SS

interface and can help understand and provide quantitative data on the dynamics occurring at various sites at the interface. STM has the potential to track single molecules on a time scale of milliseconds to hours and allows one to study the dynamics of monolayer formation on surfaces. As advances in STM continue, new doors open for investigating and understanding various surface phenomena under previously inaccessible conditions.[12-14] For example, Jahanbekam *et al.* showed that by enclosing the whole STM body in a controlled chamber one can perform temperature dependent studies on volatile solvents such as toluene (up to at least 75 °C).[12]

Distinguishing between thermodynamically and/or kinetically formed surface structures lies at the heart of understanding the SS interface.[15] A recent work by Jahanbekam *et al.*[16] has highlighted the importance of distinguishing the formation of surface structures where a kinetic product can easily be misinterpreted and treated as an equilibrium species. Although such misinterpretations have been reported in the past, researchers are becoming more cautious in their claims.[17] For surface processes that occur in a reasonable period (milli-seconds to hours), sequential STM imaging of the same area can be useful in determining whether the surface is a thermodynamic or a kinetic product. Using this sequential STM imaging technique, Friesen and co-workers successfully demonstrated that oxygen binding to cobalt(II) octaethylporphyrin at the 1-phenyloctane/highly ordered pyrolytic graphite (HOPG) interface is an equilibrium process.[18] On the other hand, sequential STM imaging studies on porphyrins have shown that monolayer formation at room temperature on HOPG and Au(111) are predominantly kinetically controlled.[19-22] On a quantitative level, temperature dependent studies can provide a vast wealth of information about the SS interface. It can provide thermodynamic quantities such as ΔG, ΔS, and ΔH,[18] and kinetic parameters such as rate constants and activation energies.[19,20] For surface structures where more than one phase is present, temperature and/or concentration dependent

studies can yield valuable information regarding the nature and stability of these phases.[23] Unless sequential STM imaging and temperature dependent studies are performed, a kinetically trapped system can easily be misinterpreted as a thermodynamically stable system. In some cases, metastable phases were identified.[17,18,24,25]

For a single component systems, the difficulty in distinguishing between thermodynamic and kinetic control is that a vacant site on the surface created by molecular desorption is very rapidly replaced by the same species in solution and hence the changes are not recognizable. To address this issue, one can use a two-component system comprised of two chemically very similar molecules that appear different under STM. Many two-component systems have appeared in the literature to address the relative stability of the adlayer at the SS interface. [17,19-23, 26,27,28] One of the earliest examples of such two-component systems dealt with a mixture of saturated and unsaturated acids and mixture of an alcohol and a thiol.[29] It was shown that the residence time of these molecules on a HOPG surface was as short as 0.03 to 0.3 s and that the exchange at the interface was rapid. Similarly, alkanes or ethers mixed with thioethers of varying lengths showed dynamic changes at the interface with residence times of up to 18 s.[30,31] Exchange dynamics of two very similar donor-acceptor-donor triads were also studied.[32] The replacement of one triad with the other at the interface occurred within minutes of addition of the second triad. Exchange halts when equilibrium is established between the surface and solution. Another similar study in an electrochemical environment was performed on a mixture of iron and free base protoporphyrins.[33] Although it was shown that the surface coverage was the same as the solution mole fraction of the porphyrins, no effort was made to study the exchange dynamics at the interface. Recently, two-component studies on porphyrins have shown that the surface structures of octaethylporphyrins are kinetically controlled at the SS interface.[19-22]

In this study, STM is used to determine and compare the desorption kinetics of a metallated porphyrin, 2,3,7,8,12,13,17,18-Octaethyl-21H,23H-porphine cobalt(II) (CoOEP) and a metal free porphyrin, 2,3,7,8,12,13,17,18-Octaethyl-21H,23H-porphine (H_2OEP) from HOPG into 1-phenyloctane at 90 °C, 100 °C, and 110 °C. Cobalt porphyrins and phthalocyanines appear brighter in an STM image compared to a metal free porphyrins and phthalocyanines.[33-37] Hence, either one of the porphyrins can be used as a tracer for surface desorption of the other at the SS interface. Here, we extend our previous studies on CoOEP desorption from Au(111)[20] and HOPG[19] to include the desorption of H_2OEP, a metal free octaethylporphyrin. These results will provide direct insights into the effect of the central metal in a porphyrin on the adsorption/desorption process from HOPG.

We will show that the rates of desorption for both porphyrins from HOPG are similar at the temperatures studied. Thus, the transition metal center has a minor impact on the stability of OEPs on HOPG. Their adsorption strength is dominated by the interaction between the porphyrin core and graphite. Furthermore, we will show that desorption from graphite step edges and grain boundaries occurs faster than from terraces.

Experimental Section:

The experimental methods employed in this study are similar to those previously reported[19,20] so attention primarily is placed on the unique aspects of the work done here.

CoOEP, often identified as cobalt octaethylporphyrin, and H_2OEP, often identified as free base octaethylporphyrin, were purchased from Aldrich and PorphyChem respectively. 1-phenyloctane (98%) was purchased from both Aldrich and Alfa Aesar and was subjected to

further purification as described elsewhere.[20] HOPG was purchased from SPI Supplies (grade-I and II) and μmasch (spread 0.8º ± 0.2º). HOPG was freshly cleaved before a new sample was prepared. These experiments are hard and time consuming, and they are made especially so by any impurities in the solvent or compounds used. Even with careful handing, the solutions tend to age resulting in "high spots' scattered around the image that we felt compromised the data and required new solutions and samples to be prepared. Most of our experimental time was spent obtaining high quality samples.

UV-Visible spectroscopy on saturated and filtered solutions of porphyrins in 1-phenyloctane was used to determine their solubility at room temperature. The measured solubility at 20 °C of CoOEP in 1-phenyloctane was 3.9×10^{-4} M or 0.23 g/L and that of H_2OEP was 1.1×10^{-4} M or 0.06 g/L. The concentration range for solutions used in these experiments was 6.4×10^{-5} M to 1.1×10^{-4} M for CoOEP, and was 5.0×10^{-5} M to 7.3×10^{-5} M for H_2OEP. Thus, all solutions were below the solubility limit.

STM images were recorded using a Molecular Imaging (now Agilent) Pico 5 STM equipped with a scanner capable of imaging a maximum area of 1 μm^2 and having an overall current sensitivity of 1 nA/V. The Agilent environmental chamber was used for all experiments and argon atmosphere was maintained. STM tips were primarily prepared by cutting and sometimes electrochemically etching. $Pt_{0.8}Ir_{0.2}$ wire was purchased from California Fine Wire Company. Images were typically obtained in constant current mode at a sample potential of +0.5 to +0.7 V and a tunneling current of 20 pA. Image sizes ranging from 35×35 nm^2 to 50×50 nm^2 were collected at a scan rate of 4.7 lines/sec, giving a total image time of just under 2 min. Images larger than 50×50 nm^2 were scanned at a slower scan rate of 3.3 to 3.9 lines/sec, giving a total image time of roughly 2.5 minutes. The temperature of the sample was controlled by a

variable-temperature hot stage using a Lakeshore 330 auto-tuning temperature controller. The environmental chamber was purged with 99.996% Ar (A-L Compressed Gases, Inc., Spokane, WA) at all times. It is important to maintain an inert atmosphere due to HOPG supported CoOEP's ability to bind O_2 from the atmosphere near room temperature.[18] The O_2-CoOEP adduct appears dim in an STM and can be misinterpreted as a H_2OEP molecule. Before imaging, samples were allowed to sit for 30 minutes to one hour inside the environmental chamber purged with Ar at 2.5 standard cubic feet per hour (scfh). During imaging, Ar was continuously purged at 0.5 scfh into the environmental chamber.

Solutions of CoOEP and H_2OEP were prepared by dissolving solid porphyrin compounds in purified 1-phenyloctane. Concentrations were measured using a UV-visible spectrophotometer where the extinction coefficient of each species had been previously measured by applying Beer's law to a series of dilutions of known concentration solutions. For CoOEP and H_2OEP the extinction coefficients were 2.179×10^5 1/cm-M and 1.61×10^5 1/cm-M, respectively. A custom-made STM solution cell was used to accommodate large volumes (up to 100 μL) of solution in contact with the HOPG surface.

Samples heated to temperatures between 20 °C and 70 °C were imaged at the indicated temperatures. At temperatures above 70 °C the drift became too large to reproducibly identify particular regions of the sample. For the higher temperatures, timed heating experiments were used. The temperature of the sample was ramped at a rate of 5 °C per minute, allowing the sample to reach the desired temperature (within the 90 °C - 110 °C range) in 20 min. The sample then was held at the desired final temperature for the desired time period. After this fixed time heating, samples were rapidly cooled to room temperature by turning the heater off. Samples were then allowed to equilibrate for at least 60 minutes prior to recording any images. The

samples never left the STM and the tip was only withdrawn sufficiently to avoid contact with the surface. All STM images were background subtracted using SPIP (www.imagemet.com) image processing software.

Tip induced desorption was seen for both porphyrins as was previously reported for CoOEP.[19] Further information on these induced desorption events is presented in the supplemental section. Whenever a tip induced desorption was observed, the scanner was moved to a new area and data collection was restarted.

STM experiments on voltage dependent desorption were also performed. Here, a monolayer of H_2OEP was first created. Then, an excess of CoOEP solution was added such that the CoOEP mole fraction in solution, X_C , equaled 0.80. The sample was then heated to 50 °C where the bias on the sample was changed to either ±1.5 V for a fixed amount of time and returned to +0.7 V (the scanning bias used to obtain all the STM images in this work) for imaging. All images were obtained at 50 °C. For all experiments where voltage changes (±1.5 V) were performed for up to 3 hours, surface coverage of CoOEP (that replaces the desorbed H_2OEP on surface) was found to be statistically the same as observed at the same temperature and time in the absence of applied bias. For all cases, the relative surface coverage of CoOEP was constant within 1.5 % to 3.0 %. Hence, any voltage dependent desorption can be ignored and the surface desorption of either octaethylporphyrin is solely due to temperature. In what follows, we will denote a generic octaethylporphyrin, independent of central species, as OEP.

Results and Discussions:

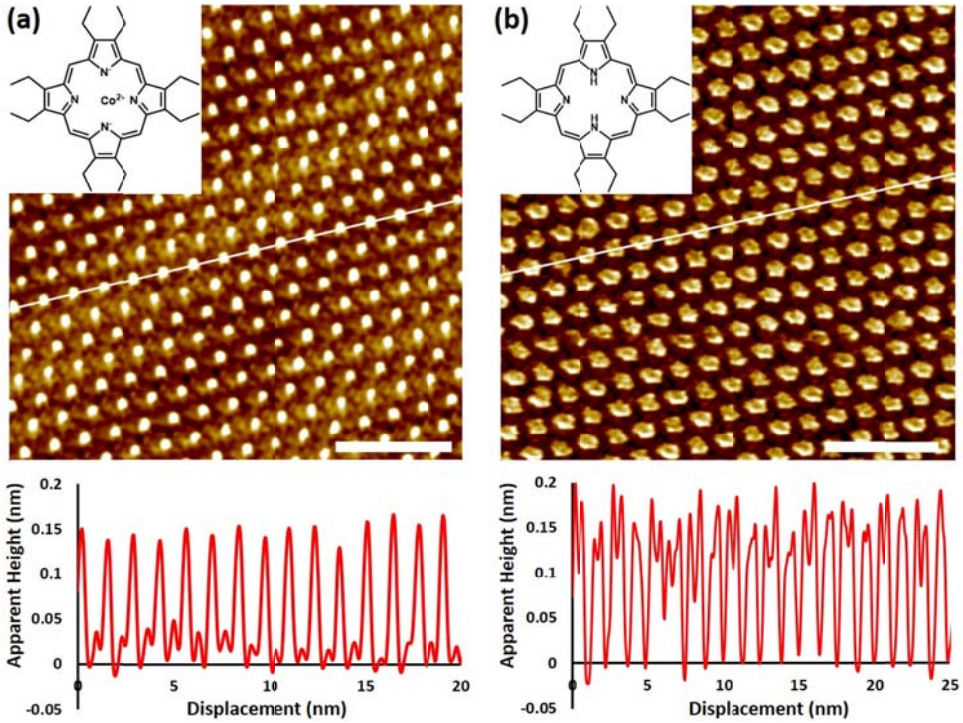

Figure 1. 20×20 nm^2 STM images at the 1-phenyloctane/HOPG interface of (a). CoOEP (only) and (b). H_2OEP (only) at a sample bias of +0.7 V and current of 20 pA. The scale bars shown are 5 nm.

Pure monolayers of CoOEP and H_2OEP on HOPG were formed by exposing freshly cleaved HOPG to individual solutions prepared in 1-phenyloctane. STM images shown in Figure 1 were taken under Ar at room temperature. Line profiles clearly indicate that the CoOEP centers appear bright whereas a depression is seen at the center of H_2OEP. A half-filled d_z^2-orbital of the cobalt ion gives rise to the brightness of the molecule, whereas the lack of states near the Fermi level in H_2OEP is responsible for the depression.[33-37] The intensities given by line profiles of an STM image can only be compared between molecules within the same image (or when the same tip is used) and hence should not be confused with the absolute height of the molecule. In any case, a solution mixture of CoOEP and H_2OEP deposited on HOPG surface

gives a mixture of clearly identifiable bright and dark sites indicative of CoOEP and H_2OEP respectively. As the solution ratio of CoOEP is increased relative to H_2OEP, the number of bright sites also increases on the HOPG surface as is shown in Figure 2. This is consistent with our expectation that CoOEP is bright and H_2OEP is dark.

Both OEP occupy similar areas on HOPG with A = 1.3 ± 0.02 nm, B = 1.4 ± 0.02 nm, and α = 57.5° ± 2° (assuming one molecule per unit cell). For NiOEP on Au(111) under UHV conditions, the ethyl groups were resolved and the unit cell was found to consist of two molecules.[38] Since we were not able to resolve the ethyl groups, the surface structure was analyzed based on one molecule per unit cell. This was done for simplicity, not because there is any evidence that the surface cells are different in vacuum versus in solution.

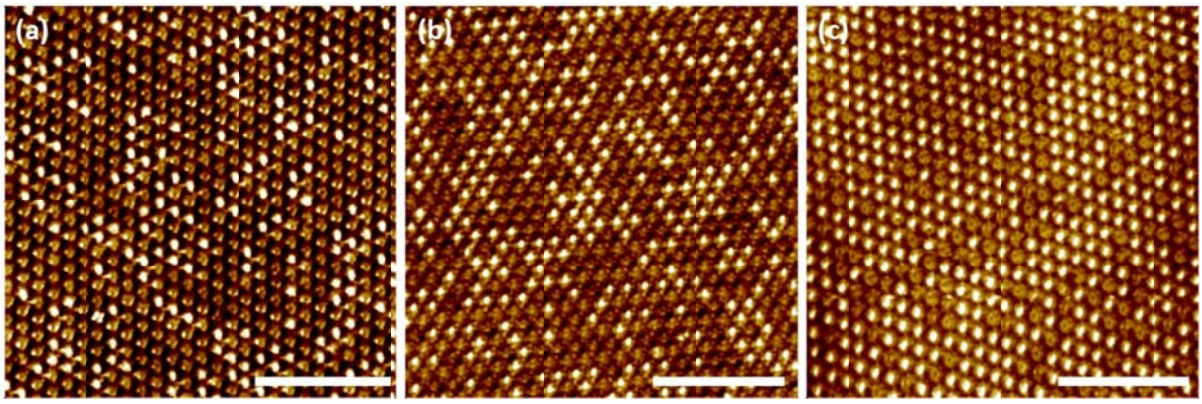

Figure 2. Room temperature STM images of mixtures of CoOEP and H_2OEP in 1-phenyloctane at the HOPG-solution interface at (a) X_C = 0.34 ± 0.03 and Θ_C = 0.32 ± 0.02, (b) X_C = 0.46 ± 0.03 and Θ_C = 0.46 ± 0.02, and (c) X_C = 0.66 ± 0.03 and Θ_C = 0.65 ± 0.01. Set point conditions: sample bias of +0.7 V and current of 20 pA. The scale bars shown are 10 nm.

Taking *M* as C for CoOEP and *M* as H_2 for H2OEP, we define X_M as the ratio of the number of *M*OEP molecules in solution to the total number of porphyrins in solution. Similarly,

Θ_M as the ratio of the number of *M*OEP to the total number of porphyrins on the surface. In both definitions, solvent molecules are excluded. Determinations of the surface coverages at room temperature produced by various relative concentrations of solution (a few examples are shown in Figure 2) yield results consistent with previous works on porphyrins: the relative surface coverage is effectively the same as the mole fraction in solution.[19,20] To determine the stability of the adlayer, temperature dependent studies and sequential STM imaging of mixed monolayers were performed. Figure 3 shows temperature dependent STM images of $X_C = 0.34 \pm 0.03$ at 25 °C, 50 °C, and 70 °C acquired at the temperatures indicated. In all three cases, Θ_C was

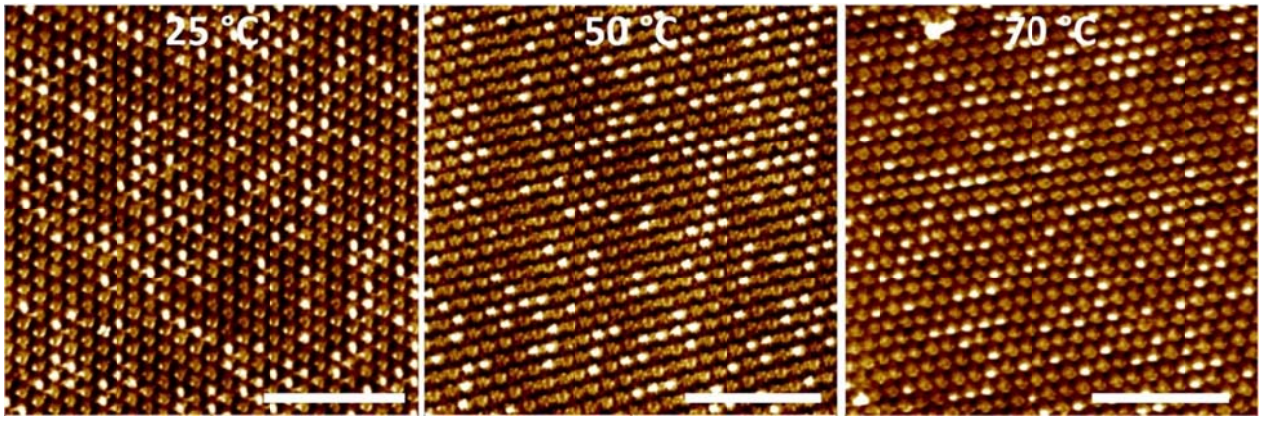

Figure 3. In-situ temperature dependent STM images of $X_C = 0.34 \pm 0.03$ and $\Theta_C = 0.32 \pm 0.04$ at 25 °C, 50 °C, and 70 °C. Set point conditions: sample bias of +0.7 V and current of 20 pA. The scale bars shown are 10 nm.

0.32 ± 0.04. Furthermore, sequential images of the same mixture at 50 °C (as depicted in Figure 4) demonstrated that the detailed molecular distribution of the monolayer does not change on a time scale of minutes. Out of many sequential images analyzed, our only indication of molecular exchange was seen in two of many images taken at 70 °C. To be more specific, only three molecules were found to exchange between the surface and solution (Figure S1). This number is extremely small compared to the total number of molecules observed over many

sequential images analyzed at 70 °C (> 7000 molecules!) and suggests that the monolayer is kinetically stable up to 70 °C.

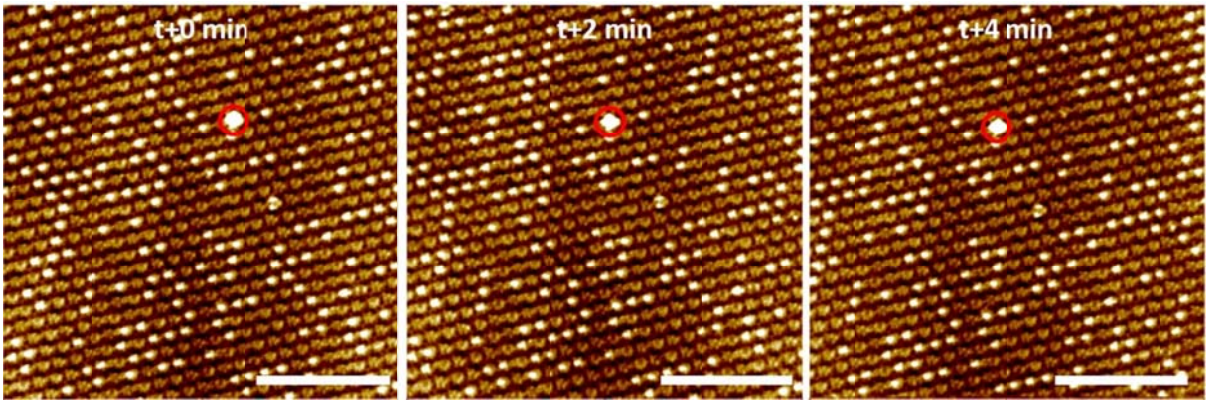

Figure 4. In-situ sequential STM images of $X_C = 0.34 \pm 0.03$ at 50 °C show no changes in the monolayer with respect to the marker indicated with a red circle. Each image is separated in time by 2 minutes. Set point conditions: sample bias of +0.7 V and current of 20 pA. The scale bars shown are 10 nm.

The fact that the surface coverage of a species is essentially the same as its solution mole ratio tells us that both the porphyrins have similar rates of adsorption. More precisely, they have very similar diffusion rates[39] and thus their sticking probabilities on the HOPG surface are similar. One can still ask, how long it takes for a complete monolayer to form. To answer this, an experiment was performed where; first, only one species of OEP was deposited. Then, it was exposed to an excess solution of the other OEP within 10 s. Imaging this perturbed system only showed the original OEP; i.e., when H_2OEP was deposited first followed by an addition of excess CoOEP, only H_2OEP was seen in the STM image (illustrated in Figure 5). Similarly, the composition of a pure CoOEP monolayer at room temperature was unchanged when the surface was exposed to the free base within a few seconds of initial CoOEP solution exposure. Hence, the monolayer formation appears to be extremely fast and forms within seconds.

Before accepting this at face value, one should ask about mixing and diffusion time, since the probe porphyrin must reach the surface before it can replace the one originally covering the surface.[40] The experiment begins with a solution layer covering the sample. The initial adsorption covers the surface with 0.065 cm of solution. The injection of the second species (tracer) is turbulent, so a thinner layer of the tracer free surface remains. As a rough estimate, we assume 1/4 of it remains. Thus, the tracer must diffuse through a layer of at least 0.02 cm before reaching the adlayer surface. Taking the diffusion time for 1 dimensional diffusion to be[41] $t = \frac{x^2}{2D}$, and computing D = 1.4×10^{-6} cm^2/s using reference 39 and 42, one finds a time of 94 seconds. Of course, diffusion is a Gaussian distribution process and some molecules will arrive sooner and many will arrive later, but this does limit our ability to specify the time for monolayer formation to less than about one minute, not the 1-10 second time frame of the injection process. It is also interesting to estimate how long monolayer formation would take if it was diffusion limited. The monolayer surface has 5.5×10^{13} molecules/cm^2 and at 10^{-4} M there are 6.0×10^{16} molecules/cm^3 in solution. This would require all molecules in a height 9.2×10^{-4} cm high. Using the same diffusion time as above, we find that the monolayer would form in about 0.3 seconds. Thus, the time window for OEP monolayer formation is between 0.3 seconds and 100 seconds.

Monolayers of both OEP's at room temperature had domain sizes in the range of hundreds of nanometers. Thus, only a handful of grain boundaries were observed. This shows that the process of monolayer formation for both porphyrins is very similar and that the cobalt ion does not have a large influence on the adsorption process on HOPG.

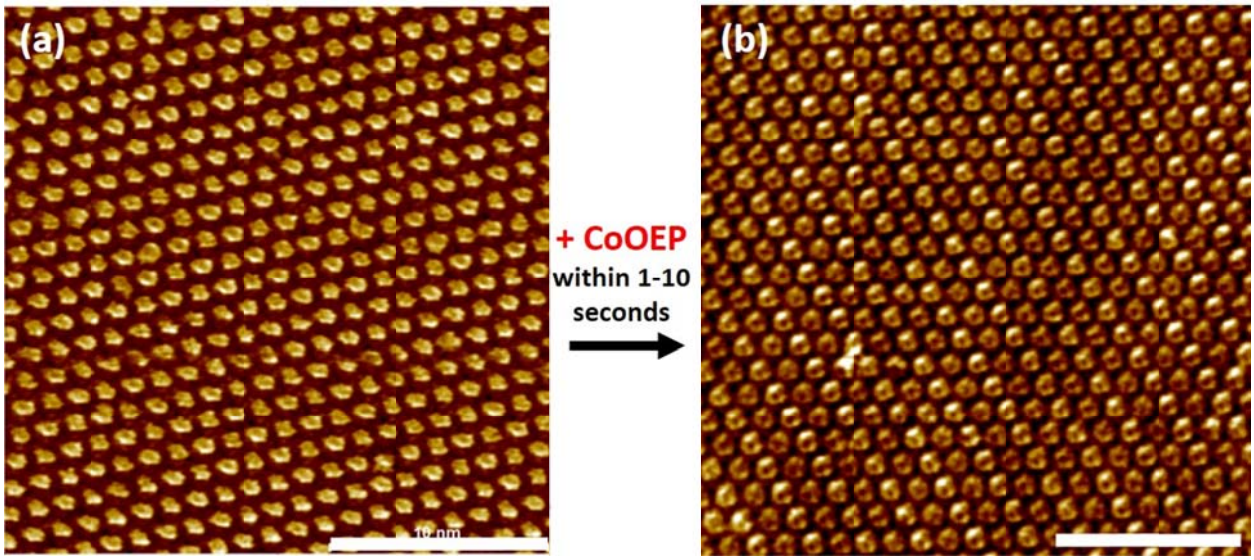

Figure 5. STM images at 25 °C of H_2OEP (a) before and (b) 24 h after the addition of CoOEP within 10 s. In both cases only H_2OEP is seen on the surface. Final X_C = 0.80. Set point conditions: sample bias of +0.7 V and current of 20 pA. The scale bars shown are 10 nm.

For adsorption of mixtures of OEP, a kinetic analysis (provided in references 19 and 20) results in the expression for relative coverage given below, where we have assumed that the rate of adsorption is orders faster than the rate of desorption.

$$\theta_C = (1 - e^{-\bar{k}Mt})\left(\frac{k_C^a X_C}{\bar{k}}\right) \qquad (1)$$

and, $$\bar{k} = \left(k_C^a X_C + k_H^a X_H\right) = k_C^a X_C + k_H^a (1 - X_C) \qquad (2)$$

where, k_C^a and k_H^a are the adsorption rate constants for CoOEP and H_2OEP respectively, and M is the total molarity of porphyrins in solution. As explained above, at lower temperatures the rate of adsorption is fast and the rate of desorption is extremely slow, so (t → ∞) and $\theta_C = \left(\frac{k_C^a X_C}{\bar{k}}\right)$.

Thus, θ_C depends only on the mole fraction and relative rates of adsorption of the OEP.[19,20] Because $\theta_C = X_C$, the rates of adsorption of the OEP's are similar.

An example of the slow desorption process at 50 °C is shown in Figure S2. Here, a monolayer of H_2OEP is initially created and exposed to a CoOEP solution such that $X_C = 0.80$. Then, the sample is heated to 50 °C and imaged at the same temperature. As can be seen from Figure S2, after 5 hr at 50 °C only 1.6 % of H_2OEP is desorbed and replaced by CoOEP. Thus, underscoring the need for studying desorption over a range of temperatures in order to determine rate parameters for the desorption process.

It is clear from the real time temperature dependent images described earlier that the desorption rates are extremely slow even at 70 °C. Gathering real time images much above 70 °C is not possible with the STM used in this study because of the very large thermal drift above about 75 °C. Hence, in order to obtain quantitative information we either need to gather images at 70 °C for at least ~15 hours (for only 15% desorption) or for at least 350 hours to achieve equilibrium; or, we can heat without scanning and then cool to image. The second process, identified as a timed heating desorption scheme, allows measurements at higher temperatures where substantial desorption of OEP from HOPG occurs within a few hours. We opted to follow the timed heating desorption scheme.

In the timed heating desorption scheme, a monolayer of either OEP is prepared. Then, an excess of the other OEP (tracer) is added to the solution such that the final mole fraction of tracer OEP in solution, X(tracer), is 0.80. As shown in Figure 5 and real time temperature dependent studies (Figure 4), the initial OEP is unlikely to desorb significantly below 70 °C. The mixture is annealed at 90 °C, 100°C, and 110 °C for time intervals of 30 min or 60 min and immediately

cooled back down to room temperature and imaged. *Due to the fast adsorption and slow desorption rates the images obtained after cooling the sample mimic the surface at the annealed temperature and time*. The choice of annealing temperature, heating rate, and cooling rate are extremely important. Choosing too high of a temperature and/or too slow a heating and cooling rate results in significant desorption during the heating and cooling; thus, the observed surface coverage value, Θ will reflect more desorption than the amount desorbed at the higher temperature. This subsequently leads to over estimating the rates. An indicator of the error caused by this procedure is the difference in coverage observed for a series of short heating times compared to the coverage seen after one long time that is equal to the sum of the individual times.

After a particular heating-hold-cool cycle, sufficient STM images were captured (up to 15,000 molecules per data point analyzed). Then the sample was annealed at the same temperature for another cycle and the process was continued for up to 4 h of total annealing time. To minimize the errors in $\Theta(t)$, some of the values determined from a series of short annealing cycles were checked against STM data obtained from images resulting from, a single annealing performed for a total time t. Representative images acquired during this study are shown in Figure 6, Hence, the $\Theta(t)$ values in Figure 7 are a collection of both the above mentioned ex-situ annealing schemes. That is, each point on the graphs in Figure 7 is the result of averaging between six and twenty images. The images used were a mix of those obtained by a single heating and those resulting from sequential heating. The uncertainty shown in Figure 7 is the actual standard deviation of the averaged values. It does not include any contributions from possible temperature error.

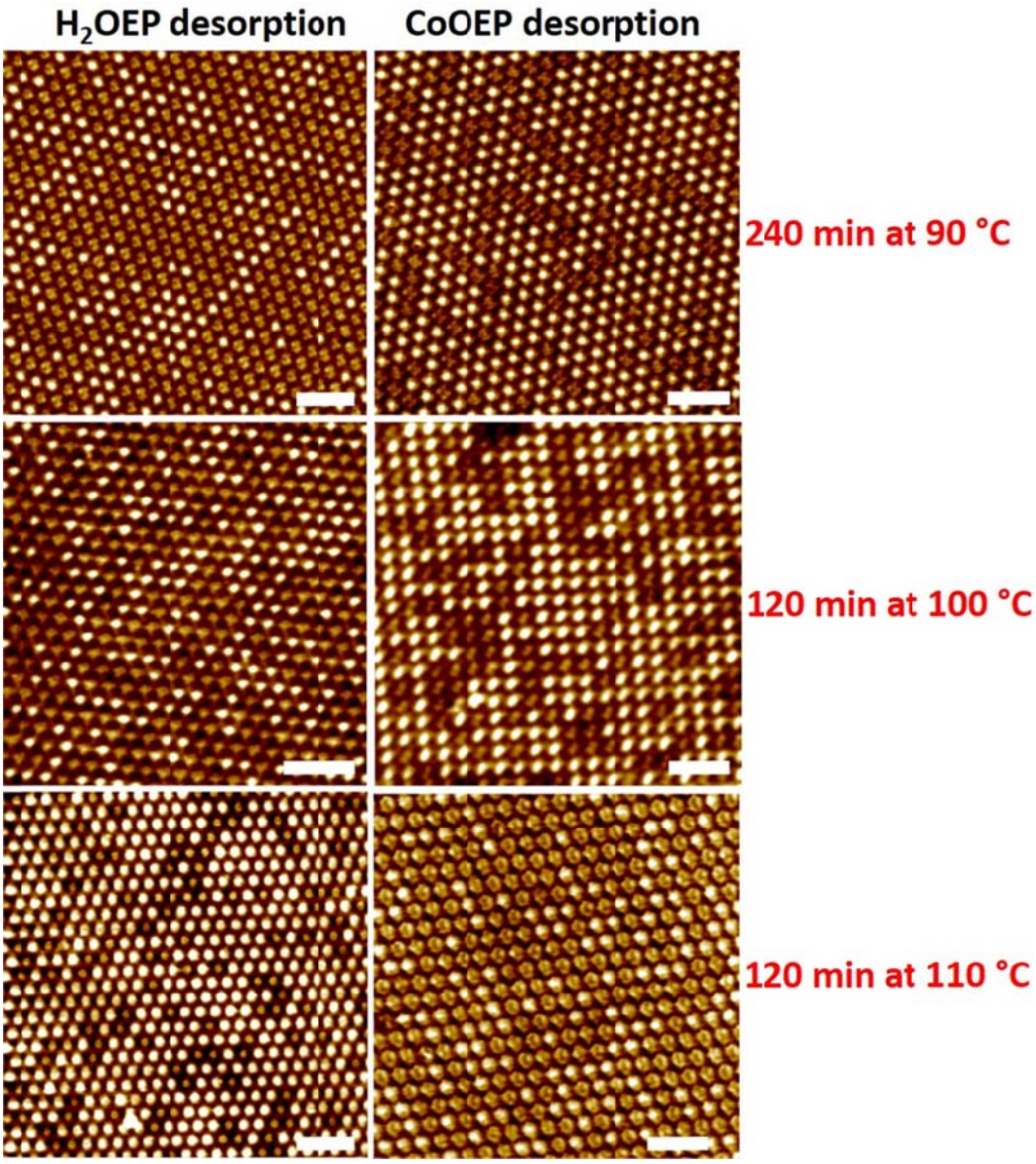

Figure 6. Representative STM images from timed desorption of OEP. Samples were initially covered with a monolayer of the compound indicated at the top, and then exposed to an X=0.8 solution of the other OEP during the heating and measuring period. All samples were heated to the indicated temperature for the indicated time then rapidly cooled to 23 °C for imaging. Set point conditions: sample bias of +0.7 V and current of 20 pA. The scale bars shown are 5 nm.

After each annealing cycle, surface coverage, $\Theta(t)$ values were collected and plotted with respect to time for each temperature given in Figure 7. In order to extract rate parameters, we used a model developed in references 19 and 20. In this model, the rate of appearance of XOEP on a complete monolayer covered by both XOEP and YOEP is equal to: {the rate of disappearance of XOEP × the probability that this vacant site will be filled by YOEP} – {the rate of disappearance of YOEP × the probability that this vacant site will be replace by XOEP}. Here, if 'X' is CoOEP then 'Y' is H_2OEP and vice-versa. This model is based on the assumption where the rates of adsorption are many orders in magnitude faster than the rates of desorption. Also, from our earlier assessment of the adsorption process, it is assumed that the rates of adsorption for both the OEP are the same, $k_H^a = k_C^a$, and that the probability of replenishing the vacant site after desorption for either OEP is the same as its mole fraction in solution, $P_i = X_i$. The following equations result from the above model:

$$\Theta_y(t) = \frac{X_y}{X_y + \mathrm{K}_x^d\left(1 - X_y\right)}\left[1 - e^{-bX_y k_x^d t}\right] \qquad (3)$$

Where, $\mathrm{K}_x^d = \frac{k_y^d}{k_x^d}$ and $b = \left[1 + \left(\left(1 - X_y\right)\left(\frac{\mathrm{K}_x^d}{X_y}\right)\right)\right]$

$\Theta_y(t)$ represents the surface coverage of the YOEP (tracer) for XOEP desorption, k_y^d denotes the desorption rate constant for YOEP, K_x^d is the relative rate of desorption of YOEP to XOEP.

Assuming an Arrhenius type desorption, equation 3 can be expanded using $k_x^d = k_x^o e^{\frac{-\Delta E_x}{RT}}$. Thus, equation 3 can be re-written as follows:

$$\Theta_y(T,t) = \frac{1}{\left[1+\left(\left(\frac{1-X_y}{X_y}\right)\left(\frac{k_x^0}{k_y^0}\right)e^{\frac{(\Delta E_x-\Delta E_y)}{RT}}\right)\right]}\left[1-\exp\left\{\left[-X_y k_x^0 e^{\frac{-\Delta E_x}{RT}}\right]\left[\left(\left(\frac{k_x^0}{k_y^0}\right)e^{\frac{(\Delta E_x-\Delta E_y)}{RT}}\left(\frac{1-X_y}{X_y}\right)\right)+1\right]t\right\}\right]$$

(4)

In equation 4, $\Theta_y(T,t)$ has four unknowns: k_x^0, k_y^0, ΔE_x, and ΔE_y. Multiple curve fitting methods can be performed using equations 3, and 4.[19] Equation 4 can be used to fit all four parameters (k_C^0, k_H^0, ΔE_C, and ΔE_H) to obtain estimated activation energies and the rate constants for desorption. In this case the uncertainties in the k^0 were very large indicating that we did not have enough data for a robust determination of all four independently. Because of this, we also tried fitting using reduced numbers of parameters. A three parameter fit based on the assumption that the attempt frequencies for desorption would be the same for both compounds: parameters $k_C^0 = k_H^0 = k^0$, ΔE_C, and ΔE_H were used. A three parameter fit assuming the desorption activation energies were the same resulted in choosing k_C^0, k_H^0, and $\Delta E_C = \Delta E_H$ as parameters. Finally, the simplest possible model where both the attempt frequencies and activation energies were the same yielded two parameters: $k_C^0 = k_H^0 = k^0$ and $\Delta E_C = \Delta E_H = \Delta E$. This last model gives the worst fit and is physically unsatisfactory since the long time high temperature steady state (equilibrium value) clearly has more H_2OEP on the surface than CoOEP (Figure 7). Table I provides all four parameters and calculated rate constants at each temperature for the curve-fitting models described above. The RMS percentage error associated with fitting all data shown in Figure 7 is also reported in Table I.

Table I. Rate parameters for both CoOEP and H_2OEP using five different curve-fitting models.

Fitting Methods	**CoOEP**						**H_2OEP**					**All**
	k_c^d **90 °C** **(hr^{-1})**	k_c^d **100 °C** **(hr^{-1})**	k_c^d **110 °C** **(hr^{-1})**	k_C^0 **(10^{13} sec^{-1})**	ΔE_C **(10^5 J/mol)**		k_H^d **90 °C** **(hr^{-1})**	k_H^d **100 °C** **(hr^{-1})**	k_H^d **110 °C** **(hr^{-1})**	k_H^0 **(10^{13} sec^{-1})**	ΔE_H **(10^5J/mol)**	**RMS % error**
4-para fit	0.096	0.29	0.84	2.7	1.25±0.04		0.14	0.46	0.84	4.2	1.25±0.04	24.0
3-para. ($k_C^0=k_H^0$)	0.096	0.28	0.84	3.5	1.26±0.04		0.13	0.40	1.14	3.5	1.25±0.04	21.2
3-para. ($\Delta E_C = \Delta E_H$)	0.12	0.37	1.08	3.3	1.25±0.03		0.15	0.46	1.32	4.1	1.25±0.03	22.6
2-para. (k^o,ΔE)	0.12	0.37	1.08	2.1	1.24±0.05		0.12	0.37	1.08	2.1	1.24±0.05	27.2
Avg.	0.11	0.33	0.96	2.94	1.25		0.14	0.42	1.13	3.54	1.25	

From Table I, it is clear that the desorption energy remains relatively constant and nearly the same for CoOEP and H_2OEP with ΔE = (1.25 ± 0.05)×10^2 kJ/mol. The pre-exponential factors are of the order of 3×10^{13} /s. Figure 7 shows the best fit curves for the 3 parameter (k_C^0=k_H^0=k^0, ΔE_C, and ΔE_H) model that has the lowest % error. Given the differences in desorption kinetics (individual rates), we tend to think that the CoOEP desorption energy is slightly greater than for the free base. However, the uncertainties in the calculated activation energies are such that one cannot with confidence attribute the rate differences solely to a difference in activation energy.

In a computational study, Chilukuri and coworkers[43] show that the CoOEP adsorption on Au(111) results in an increased density of states near the Fermi energy. This new state was attributed to cobalt ion interaction with the Au(111) surface. In the same study, no such states were found for the case of CoOEP adsorbed on HOPG, indicative of minimal or no interaction between the central metal and the HOPG surface. Their computational study is consistent with our experimental observations that the adsorption strength of CoOEP on HOPG is similar to that of H_2OEP on HOPG.

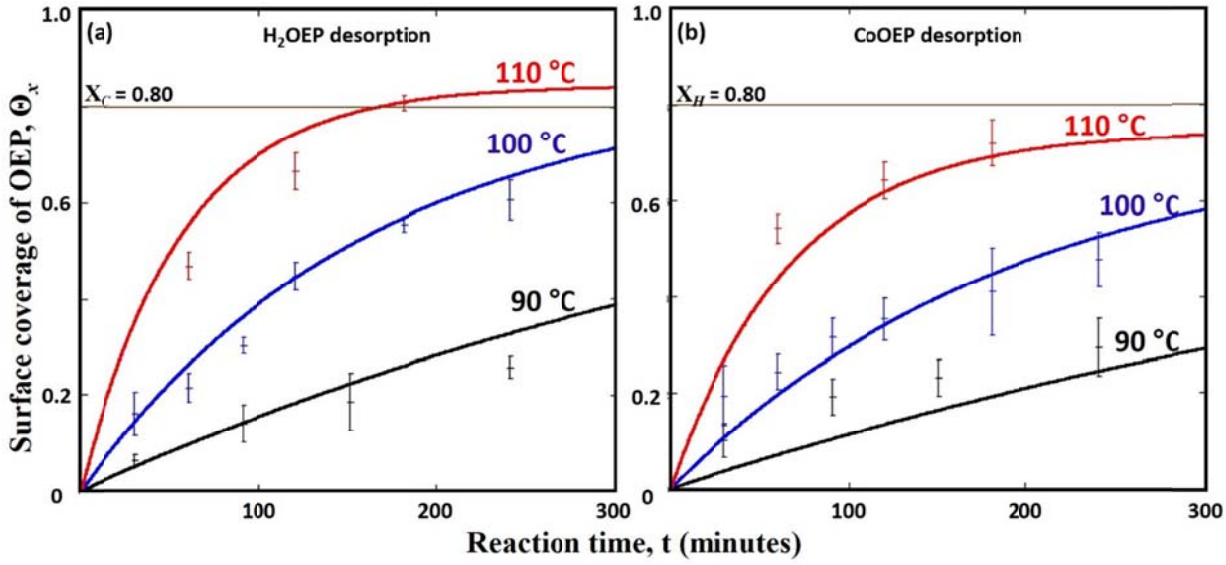

Figure 7. Three parameter best fit curves for desorption rates using equation 4 with $k_C^0 = k_H^0 = 3.5\times10^{13}$ sec^{-1}, $\Delta E_C = (1.26 \pm 0.04)\times10^2$ kJ/mol, and $\Delta E_H = (1.25 \pm 0.04)\times10^2$ kJ/mol for (a) H_2OEP at 90 °C (black), 100 °C (blue), and 110 °C (red), and (b) CoOEP at 90 °C (black), 100 °C (blue), and 110 °C (red).

The above analysis of the data shown in Figure 7 allows us to compare the rates of desorption of CoOEP in this study versus a previous work given in reference 19. In the previous work, NiOEP was used as a tracer for the CoOEP desorption whereas, H_2OEP is used in this work with similar experimental parameters. Table II provides the rate constants for CoOEP desorption when NiOEP or H_2OEP was used as tracer. It is important to note that all these studies were conducted with the same solvent (1-phenyloctane) since changes in solvent can have a significant effect on desorption energies.[44] Based on the data in Table II, CoOEP desorbs faster in the presence of NiOEP than in presence of H_2OEP from HOPG. On careful analysis of the initial desorption process, it appears that the initial surface coverage of tracer (NiOEP or H_2OEP) is independent of tracer. Stated differently, the rate of desorption of CoOEP is initially

independent of which tracer is used. After 30 min of annealing at 90 °C, with NiOEP, Θ_N (30) = 0.11 ± 0.04, and with H_2OEP, Θ_H (30) = 0.11 ± 0.04. These values are essentially the same. However, as desorption of CoOEP progresses, the surface coverage of NiOEP increases more rapidly than that of H_2OEP. This can be explained as a cooperativity effect. As the surface coverage of tracer increases, CoOEP is more likely to desorb from the surface. This situation was first described in a simple mathematical model by Temkin,[45,46] where the heat of adsorption changes as $(1+\alpha*\theta_2)$, where the heat of adsorption for the 1st component near $\theta_2 = 0$ is ΔH_1^0 and it changes smoothly to $(1+\alpha)\Delta H_1^0$ as θ_2 moves to 1. Here $\alpha \sim -0.16$. If $|\alpha|$ is large we expect significant clustering of tracer molecules as the adsorption progresses, as was seen by De Feyter.[47] If α is small, as here, the clustering may not be easily observed. Here $\alpha \sim -0.16$. We are in the process of converting these images to simple binary intensity distributions for nearest neighbor analysis.

Table II. Comparison of desorption from HOPG rate constants for CoOEP when H_2OEP was used as a tracer (this work) and when NiOEP was used as a tracer (reference 19).

rate constants for CoOEP desorption, k_C^d (min^{-1})	when H_2OEP is used as a tracer	when NiOEP is used as a tracer[19]
90 °C	0.0022 ± 0.0008	0.0055 ± 0.0007
100 °C	0.0047 ± 0.001	0.013 ± 0.001
110 °C	0.017 ± 0.008	0.033 ± 0.003

If CoOEP surrounded by NiOEP is less stable than when surrounded by either H_2OEP, the rates for CoOEP desorption using NiOEP as a tracer will be greater than when H_2OEP is used, as is seen in the data of Table II. It is also useful to note that the fitting procedure used assumes that the desorption energy is independent of coverage, and this would only be a first approximation if the desorption energy is coverage dependent. This may explain why CoOEP had a somewhat small overall desorption activation energy when replaced by NiOEP at high concentration. Also, the assumption of a coverage independent activation energy could contribute to the roughly 22% RMS error in the fits since, for example, the overall coverage at 90 °C is much less (with a larger ΔH_1) than at 110 °C (where ΔH_1 is smaller).

It is worth comparing desorption energies in vacuum with these in solution on Au(111) and on HOPG. In the case of CoOEP desorption from Au(111), only the rate constant for desorption at 135 °C was reported[19] : 4.0×10^{-3}/min. Assuming k_c^0 for graphite is similar to the value for gold, the desorption activation energy for CoOEP from Au(111) can be estimates as 138 kJ/mole. An order of magnitude increase in k_c^0 only increases the activation energy to 148 kJ/mole. While these value are higher than for HOPG, they are not as large as predicted by DFT calculations where a difference in vacuum desorption energies between HOPG and Au(111) of as much as 180 kJ/mole is reported.[43] While the DFT calculations may have exaggerated the difference in the HOPG and Au(111) surfaces, it is also possible that much of the difference between measured solution and calculated vacuum desorption energies arises from solvent interactions. As Lackinger and coworkers have shown,[48] the energy of desorption in solution contains terms for the solvation of the adsorbate, the wetting of graphite by the solvent, the

wetting of the monolayer by solvent, the sublimation energy of the adsorbate, and the heat of adsorption in vacuum. For the same adsorbate and solvent, the wetting terms and the vacuum desorption energy are the only ones that change with substrate. The heat of wetting of an OEP monolayer is unknown, but is expected to be similar whether supported on gold or HOPG since the monolayer densities are essentially the same (1.57±0.08 nm^2 on Au(111)[20] and 1.50±0.08 nm^2 on HOPG). Thus, the critical solution property is the heat of wetting of the clean substrate. For graphite, the heats of wetting by a wide range of hydrocarbons fall within the range of -110 erg/cm^2 to -130 erg/cm^2.[49,50] The heat of wetting of Au(111) by 1-phenyloctane is not available. But, polycrystalline newly synthesized and reduced copper is reported to have a heat of wetting of the order of 700 erg/cm^2 for most organic systems,[50] but to decrease to more than 200 erg/cm^2 depending on preparation. Taking the adsorption area of 1-phenyloctane to be 6.2×10^{-15} cm^2, the heat of wetting for 1-phenyloctane on HOPG is 45 kJ/mole, and on copper it ranges from about 260 kJ/mole to 75 kJ/mole, depending on the copper preparation. If the heats of wetting of Au(111) are of the same magnitude as for copper, than the vacuum desorption energies could be as much as 180 kJ/mole greater for Au(111) than for HOPG. This example highlights the need for good thermodynamic values for heats of wetting and vacuum desorption energies for single crystal surfaces.

Desorption from step edges and grain boundaries

All of the above analysis for the kinetics of desorption for OEP applies to desorption from terraces of HOPG. It has been well documented in the past that the kinetics of adsorption and desorption can be different along step edges and grain boundaries.[51,52] High catalytic activity along step edges[53] and molecular exchange mechanisms through grain boundaries have also been reported.[54] In a similar experiment concerning NiOEP desorption from Au(111) at the

1-phenyloctane/Au(111) interface, it was shown that NiOEP preferentially desorbs from step edges and reconstruction lines.[20] In this work we observed preferential desorption of H_2OEP from step edges and grain boundaries. CoOEP was not observed to show preferential desorption from step edges. Since single domains of OEP on HOPG extend to hundreds of nanometers in size, few grain boundaries were observed during CoOEP desorption and hence we leave this analysis for future work.

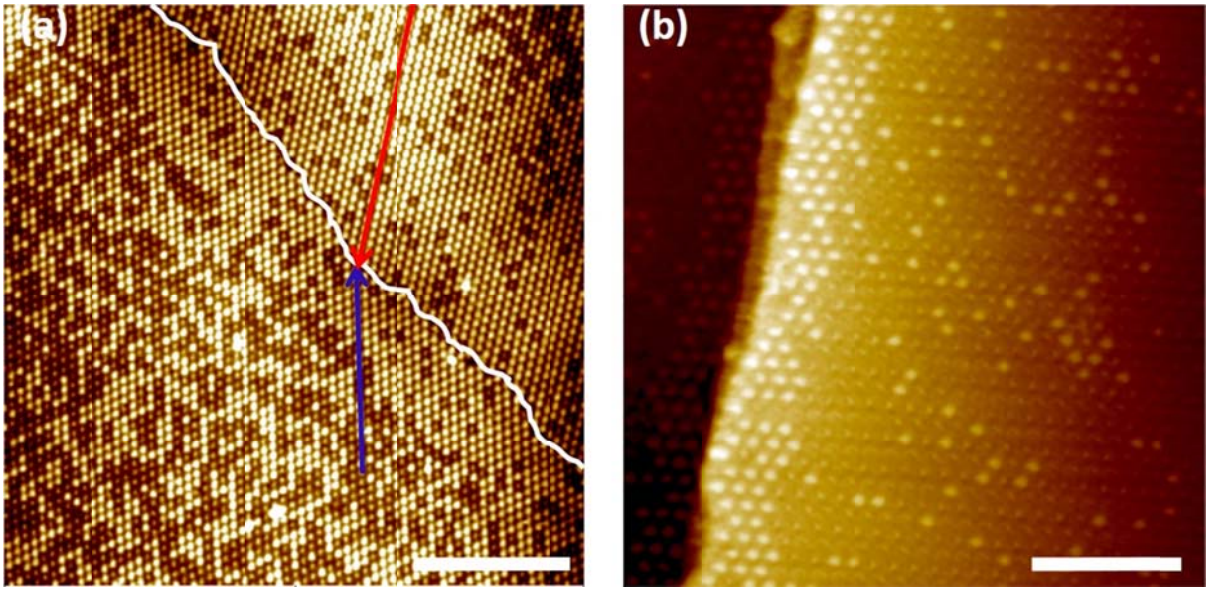

Figure 8. STM images of site specific desorption. (a) Desorption from a grain boundary: H_2OEP desorption after 30 min at 110 °C shows higher surface coverage of CoOEP (bright sites) along the grain boundary shown by the white curve. Red and blue lines show two different lattice directions separated by the grain boundary. The scale bar shown is 20 nm. (b) Desorption from a step edge: H_2OEP desorption after 90 min at 90 °C shows higher surface coverage of CoOEP (bright sites) close to the step edge. The scale shown is 10 nm. In both images, set point conditions used are 0.7 V and 20 pA tunneling current.

Conclusions

Desorption kinetic parameters of CoOEP and H_2OEP at the solution/solid interface have been determined using STM. At temperatures below 70 °C, monolayers of OEP on HOPG are controlled by kinetics and the rates of desorption are extremely slow. Significant desorption and eventual equilibration between the surface and solution in a time scale of hours occurs at 90 °C, 100 °C, and 110 °C. The rates of desorption and the desorption activation energies for H_2OEP and CoOEP on HOPG are very similar and show only weak effects due to the presence of cobalt ion. Thus, the adsorption strength most likely arises from the interactions between the porphyrin core and the HOPG surface. The desorption activation energy is (125±5) kJ/mol. When compared to an earlier study of CoOEP desorption from HOPG (with NiOEP as a tracer), the overall activation energy for OEP desorption from HOPG into 1-phenyloctane can be given as 105 – 130 kJ/mol. In the case of CoOEP desorption from Au(111), assuming k^0 for gold is similar to the value for HOPG, the desorption activation energy for CoOEP from Au(111) is ~138 kJ/mole. The small difference in solution phase desorption energies from Au(111) and HOPG compared to the large predicted difference in vacuum is attributed to differences in wetting of the HOPG and Au(111) surface. Voltage dependent desorption experiments show that the stability of monolayers of OEPs is not affected by the substrate potential relative to ground but that changes in substrate-tip potential can modify desorption rates.

Although solubility values for both OEP are different, the concentrations used to perform all the experiments are significantly lower than their solubility limits. It is suggested that the difference in desorption rates observed for CoOEP when using different tracers (H_2OEP or NiOEP) is the result of a (anti-) cooperativity. That is, the desorption activation energies reported here and in the NiOEP tracer study may be slightly different than for a pure CoOEP layer.

H_2OEP was found to preferentially desorb from HOPG at step edges and grain boundaries. This behavior is similar to that observed for NiOEP on Au(111). Further studies of these site specific desorption processes are underway.

ACKNOWLEDGEMENT

We thank the US National Science Foundation for their support in the form of grant CHE-1403989.

ASSOCIATED CONTENT

Supplemental material contains STM images at elevated temperatures, and images relating to sample bias and sample-tip voltage induced surface changes. This material is available free of charge via the Internet at http://pubs.acs.org

References

[1] Yokoyama, T.; Yokoyama, S.; Kamikado, T.; Okuno, Y.; Mashiko, S. Selective Assembly on a Surface of Supramolecular Aggregates with Controlled Size and Shape. *Nature* **2001**, *413*, 619-621.

[2] Adisoejoso, J.; Tahara, K.; Lei, S.; Szabelski, P.; Rzysko, W.; Inukai, K.; Blunt, M. O.; Tobe, Y.; De Feyter, S. One Building Block, Two Different Nanoporous Self-Assembled Monolayers: A Combined STM and Monte Carlo Study. *ACS Nano* **2012**, *6*, 897-903.

[3] Hayashi, H.; Higashino, T.; Kinjo, Y.; Fujimori, Y.; Kurotobi, K.; Chabera, P.; Sundström, V.; Isoda, S.; Imahori, H. Effects of Immersion Solvent on Photovoltaic and Photophysical Properties of Porphyrin-Sensitized Solar Cells. *ACS Appl. Mater. Interfaces* **2015**, *7*, 18689-18696.

[4] Cristaldi, D. A.; Capuano, R.; D'Urso, A.; Randazzo, R.; Paolesse, R.; Di Natale, C.; Purrello, R.; Fragalà, M. E. Spontaneous Deposition of Porphyrin-Based Layers on Polylysinated Substrates: Role of the Central Metal on Layer Structural and Sensing Properties. *J. Phys. Chem. C* **2016**, *120*, 724-730.

[5] Çapan, İ; Özkaya, C. Characterization of Octaethyl Porphyrin Thin Films with Application to Determination of Volatile Organic Compounds. *Anal. Lett.* **2016**, *49*, 423-432.

[6] Qu, K.; Xu, H.; Zhao, C.; Ren, J.; Qu, X. Amine-linker Length Dependent Electron Transfer between Porphyrins and Covalent Amino-modified Single-walled Carbon Nanotubes. *RSC Adv.* **2011**, *1*, 632-639.

[7] Arai, T.; Nobukuni, S.; Sandanayaka, A. S. D.; Ito, O. Zinc Porphyrins Covalently Bound to the Side Walls of Single-Walled Carbon Nanotubes via Flexible Bonds: Photoinduced Electron Transfer in Polar Solvent. *J. Phys. Chem. C* **2009**, *113*, 14493-14499.

[8] Huber, M. The Role of the Electronic Structure of the Porphyrin as Viewed by EPR/ENDOR Methods in the Efficiency of Biomimetic Model Compounds for Photosynthesis. *Eur. J. Org. Chem.* **2001**, 4379-4389.

[9] Piatkowski, P.; Martin, C.; di Nunzio, M. R.; Cohen, B.; Pandey, S.; Hayse, S.; Douhal, A. Complete Photodynamics of the Efficient YD2-o-C8-Based Solar Cell. *J. Phys. Chem. C* **2014**, *118*, 29674-29678.

[10] Kay, A.; Grätzel, M. Artificial Photosynthesis. 1. Photosensitization of TiO_2 Solar Cells with Chlorophyll Derivatives and Related Natural Porphyrins. *J. Phys. Chem.* **1993**, *97*, 6272-6277.

[11] Li, L.; Diau, E. W. Porphyrin-sensitized Solar Cells. *Chem. Soc. Rev.* **2013**, *42*, 291-304.

[12] Jahanbekam, A.; Mazur, U.; Hipps, K. W. A New Variable Temperature Solution-Solid Interface Scanning Tunneling Microscope. *Rev. Sci. Instrum.* **2014**, *85*, 103701.

[13] Herbschleb, C. T.; van der Tuijn, P. C.; Roobol, S. B.; Navarro, V.; Bakker, J. W.; Liu, Q.; Stoltz, D.; Cañas-Ventura, M. E.; Verdoes, G.; van Spronsen, M. A. et. al. The Reactor STM: Atomically Resolved Scanning Tunneling Microscopy under High-Pressure, High-Temperature Catalytic Reaction Conditions. *Rev. Sci. Instrum.* **2014**, *85*, 083703.

[14] Perdigão, L. M. A.; Saywell, A. Haptic-STM: A Human-in-the-loop Interface to a Scanning Tunneling Microscope. *Rev. Sci. Instrum.* **2011**, *82*, 073704.

[15] Gutzler, R.; Cardenas, L.; Rosei, F. Kinetics and Thermodynamics in Surface-Confined Molecular Self-Assembly. *Chem. Sci.* **2011**, *2*, 2290-2300.

[16] Jahanbekam, A.; Chilukuri, B.; Mazur, U.; Hipps, K. W. Kinetically Trapped Two-Component Self-Assembled Adlayer. *J. Phys. Chem. C* **2015**, *119*, 25364-25376.

[17] Mazur, U.; Hipps, K. W. Kinetic and Thermodynamic Processes of Organic Species at the Solution–solid Interface: The View through an STM. *Chem. Commun.* **2015**, *51*, 4737-4749.

[18] Friesen, B. A.; Bhattarai, A.; Mazur, U.; Hipps, K. W. Single Molecule Imaging of Oxygenation of Cobalt Octaethylporphyrin at the Solution/Solid Interface: Thermodynamics from Microscopy. *J. Am. Chem. Soc.* **2012**, *134*, 14897-14904.

[19] Bhattarai, A.; Mazur, U.; Hipps, K. W. Desorption Kinetics and Activation Energy for Cobalt Octaethylporphyrin from Graphite at the Phenyloctane Solution-Graphite Interface: An STM Study. *J. Phys. Chem. C* **2015**, *119*, 9386-9394.

[20] Bhattarai, A.; Mazur, U.; Hipps, K. W. A Single Molecule Level Study of the Temperature-Dependent Kinetics for the Formation of Metal Porphyrin Monolayers on Au(111) from Solution. *J. Am. Chem. Soc.* **2014**, *136*, 2142-2148.

[21] Coenen, M. J. J.; Khoury, T.; Crossley, M. J.; Hendriksen, B. L. M.; Elemans, J. A. A. W.; Speller, S. Nanostructuring of Self-Assembled Porphyrin Networks at a Solid/liquid Interface: Local Manipulation under Global Control. *ChemPhysChem* **2014**, *15*, 3484-3488.

[22] Coenen, M. J. J.; Cremers, M.; den Boer, D.; van den Bruele, F. J.; Khoury, T.; Sintic, M.; Crossley, M. J.; van Enckevort, W. J. P.; Hendriksen, B. L. M.; Elemans, J. A. A. W. et al. Little Exchange at the Liquid/solid Interface: Defect-Mediated Equilibration of Physisorbed Porphyrin Monolayers. *Chem. Commun.* **2011**, *47*, 9666-9668.

[23] Blunt, M. O.; Adisoejoso, J.; Tahara, K.; Katayama, K.; Van der Auweraer, M.; Tobe, Y.; De Feyter, S. Temperature-Induced Structural Phase Transitions in a Two-Dimensional Self-Assembled Network. *J. Am. Chem. Soc.* **2013**, *135*, 12068-12075.

[24] Ferreira, Q.; Bragança, A.M.; Moura, N.M.M.; Faustino, M.A.F.; Alcácer, L.; Morgado, J. Dynamics of Porphyrin Adsorption on Highly Oriented Pyrolytic Graphite Monitored by Scanning Tunneling Microscopy at the Liquid/solid Interface. *Appl. Surf. Sci.* **2013**, *273*, 220-225.

[25] Piot, L.; Marchenko, A.; Wu, J.; Müllen, K.; Fichou, D. Structural Evolution of Hexa-*peri*-hexabenzocoronene Adlayers in Heteroepitaxy on *n*-Pentacontane Template Monolayers. *J. Am. Chem. Soc.* **2005**, *127*, 16245-16250.

[26] Otsuki, J.; Kawaguchi, S.; Yamakawa, T.; Asakawa, M.; Miyake, K. Arrays of Double-Decker Porphryins on Highly Oriented Pyrolytic Graphite. *Langmuir* **2006**, *22*, 5708-5715.

[27] Ikeda, T.; Asakawa, M.; Goto, M.; Miyake, K.; Ishida, T.; Shimizu, T. STM Observation of Alkyl-Chain-Assisted Self-Assembled Monolayers of Pyridine-Coordinated Porphyrin Rhodium Chlorides. *Langmuir* **2004**, *20*, 5454-5459.

[28] Yablon, D. G.; Ertas, D.; Fang, H.; Flynn, G. W. An STM Investigation of the Adsorption of Mixtures of Fatty Acids and Substituted Acids at the Solution-Graphite Interface. *Isr. J. Chem.* **2003**, *43*, 283-392.

[29] Stevens, F; Beebe, T. P., Jr. Dynamical Exchange Behavior in Organic Monolayers Studied by STM Analysis of Labeled Mixtures. *Langmuir* **1999**, *15*, 6884-6889.

[30] Padowitz, D. F.; Sada, D. M.; Kemer, E. L.; Dougan, M. L.; Xue, W. A. Molecular Tracer Dynamics in Crystalline Organic Films at the Solid-Liquid Interface. *J. Phys. Chem. B* **2002**, *106*, 593-598.

[31] Padowitz, D. F.; Messmore, B. W. STM Observations of Exchange Dynamics at the Solid-Liquid Interface Using a Molecular Tracer. *J. Phys. Chem. B* **2000**, *104*, 9943-9946.

[32] Uji-I, H.; Miura, A.; Schenning, A.; Meijer, E. W.; Chen, Z.; Würthner, F.; De Shryver F. C.; Van der Auweraer, M.; De Feyter, S. Scanning Tunneling Microscopy and Spectroscopy of Donor-Acceptor-Donor triads at the Liquid/Solid Interface. *ChemPhysChem* **2005**, *6*, 2389-2395.

[33] Tao, N. J. Probing Potential-Tuned Resonant Tunneling through Redox Molecules with Scanning Tunneling Microscopy. *Phys. Rev. Lett.* **1996**, *76*, 4066-4069.

[34] Hipps, K. W.; Scudiero, L.; Barlow, D. E.; Cooke, M. P. Jr. A Self-Organized 2-Dimensional Bifunctional Structure Formed by Supramolecular Design. *J. Am. Chem. Soc.* **2002**, *124*, 2126-2127.

[35] Barlow, D. E.; Scudiero, L.; Hipps, K. W. Scanning Tunneling Microscopy Study of the Structure and Orbital-Mediated Tunneling Spectra of Cobalt(II) Phthalocyanine and Cobalt(II) Tetraphenylporphyrin on Au(111): Mixed Composition Films. *Langmuir* **2004**, *20*, 4413-4421.

[36] Scudiero, L.; Barlow, D. E.; Hipps, K. W. Physical Properties and Metal Ion Specific Scanning Tunneling Microscopy Images of Metal(II) Tetraphenylporphyrins Deposited from Vapor onto Gold(111). *J. Phys. Chem. B* **2000**, *104*, 11899-11905.

[37] Bai, Y.; Buchner, F.; Kellner, I.; Schmid, M.; Vollnhals, F.; Steinrück, H.; Marbach, H.; Gottfried, J. M. Adsorption of Cobalt (II) octaethylporphyrin and 2H-octaethylporphyrin on Ag(111): New Insight into the Surface Coordinative Bond. *New J. Phys.* **2009**, *11*, 125004.

[38] Scudiero, L.; Barlow, Dan E.; Hipps, K. W. Scanning Tunneling Microscopy, Orbital-Mediated Tunneling Spctroscopy, and Ultraviolet Photoelectron Spectroscopy of Nickel(II) Octaethylporphyrin Deposited from Vapor. *J. Phys. Chem. B* **2002**, *106*, 996-1003.

[39] da Costa, V. C. P.; Ribeiro, A. C. F.; Sobral, A.; Lobo, V. M. M.; Annunziata, O.; Santos, C.; Willis, S. A.; Price, W. S.; Esteso, M. A. *J. Chem. Thermodyn.* **2012,** *47*, 312-319.

[40] Jung, L.; Campbell, C. T. Sticking Probabilities in Adsorption of Alkanethiols from Liquid Etanol Solution onto Gold. *J. Phys. Chem. C* **2000**, 104, 11168-11178.

[41] Berg, C. Random Walks in Biology; Princeton University Press: Princeton NJ, 1983; pp 6-16.

[42] Katritzky, A.; Chen, K.; Wang, Y.; Karelson, M.; Lucic, B.; Trinajstic, N.; Suzuki, T.; Schuurmann, G. Prediction of liquid viscosity for organic compounds by a quantitative structure-property relationship. *J. Phys. Org. Chem*. **1999**, *13*, 80-86.

[43] Chilukuri, B.; Mazur, U.; Hipps, K. W. Effect of Dispersion on Surface Interactions of Cobalt(II) octaethylporphyrin Monolayer on Au(111) and HOPG(0001) Substrates: A Comparative First Principles Study. *Phys. Chem. Chem. Phys.* **2014**, *16*, 14096-14107.

[44] Song, W.; Martsinovich, N.; Heckl, W. M.; Lackinger, M. Thermodynamics of Halogen Bonded Monolayer Self-Assembly at the Liquid-Solid Interface. *Chem. Commun.* **2014**, *50*, 13465-13468.

[45]Temkin, M.;. Pyzhev, V., Recent Modifications to Langmuir Isotherms. *Acta Physiochim. URSS* **1940**, *12*, 217-225.

[46] Foo, K.; Hameed, B. Insights into the modeling of adsorption isotherm systems. *Chem. Eng. J.* **2010**, *156*, 2-10.

[47] Mali, K.; Zçphel, L.;Ivasenko, Mullen, K.; De Feyter, S. Manifestations of Non-Planar Adsorption Geometries of Lead Pyrenocyanine at the Liquid-Solid Interface. *Chem-Asian J* **2013**, *8*, 2497-2505.

[48] Song, W.; Martsinovich, N.; Heckl, W.; Lackinger, M. Born−Haber Cycle for Monolayer Self-Assembly at the Liquid−Solid Interface: Assessing the Enthalpic Driving Force. *J. Am. Chem. Soc.* **2013**, *135*, 14854-14862.

[49] Good, R.; Girifalco, L.; Kraus, G. A Theory for Estimation of Interfacial Energies II: Application to Surface Thermodynamics of Teflon and Graphite. *J. Phys. Chem.* **1958**, *62*, 1418-1421

[50] Bartell, F.; Suggitt, R. Heat of Wetting of Copper, Graphite, and Silica Gell. *J. Phys. Chem.* **1954**, *58*, 36–40.

[51] Tierney, H. L.; Jewell, A. D.; Baber, A. E.; Iski, E. V.; Sykes, E. C. H. Dynamics of Molecular Adsorption and Rotation on Nonequilibrium Sites. *Langmuir* **2010**, *26*, 15350-15355.

[52] Wouters, D.; Höppener, S.; Lunkwitz, R.; Chi, L.; Fuchs, H.; Schubert, U. S. Highly Ordered Self-Assembled Architectures of Modified Terpyridines on Highly Ordered Pyrolitic Graphite Imaged by Scanning Tunneling Microscopy. *Adv. Funct. Mater.* **2003**, *13*, 277-280.

[53] Kim, J.; Noh, M. C.; Doh, W. H.; Park, J. Y. Thermal Evolution and Instability of CO-Induced Platinum Clusters on the Pt(557) Surface at Ambient Pressure. *J. Am. Chem. Soc.* **2016**, *138*, 1110-1113.

[54] Hohman, J. N.; Thomas, J. C.; Zhao, Y.; Auluck, H.; Kim, M.; Vijselaar, W.; Kommeren, S.; Terfort, A.; Weiss, P. S. Exchange Reactions between Alkanethiolates and Alkaneselenols on Au{111}. *J. Am. Chem. Soc.* **2014**, *136*, 8110-8121.